Förster, M., Feldstein, Y. I., Dremukhina, L. A., Levitin, A. E., Haaland, S. E. (2013): Some aspects of modelling the high-latitude ionospheric convection from Cluster/EDI data. - Geomagnetism and Aeronomy, 53, 1, 85-95,

DOI: 10.1134/S001679321301009X

Some aspects of modelling the high-latitude ionospheric convection from Cluster/EDI data

M. Förster

GFZ German Research Centre for Geosciences, Helmholtz-Zentrum Potsdam, 14473 Potsdam, Germany

Y. I. Feldstein, L. I. Gromova, *
L. A. Dremukhina, and A. E. Levitin

IZMIRAN, Troitsk, Moscow region, Russia

S. E. Haaland [1]

Max-Planck-Institut für Sonnensystemforschung, Lindau-Katlenburg, Germany

Abstract

Measurements onboard the Cluster satellites are briefly described, which form the base for determining the intensity and direction of the electric field in the magnetosphere. We discuss 1) the methodology of calculation the potential distribution at ionospheric level; 2) the results of constructing spatio-temporal convection pattern for different orientations of the IMF vector in the GSM y-z-plane (Fig. 1); 3) the derivation of Basic Convection Patterns (BCPs, Fig. 2), which allow to deduce the statistical ionospheric convection pattern at high latitudes for any values of IMF B_z and B_y (convection model); 4) the consequences of enlarging the amount of data used for the analysis; 5) the results of potential calculations with various orders of the spherical harmonics describing them; 6) the determination of the cross-polar cap potential with different IMF sector widths (from 45° down to 10°); and finally, 7) the results of our trials to determine the contribution of the IMF B_x component to the convection pattern.

Key words: magnetospheric convection, IMF dependence, Electron Drift Instrument (EDI) on Cluster

* Corresponding author
Email addresses: mfo@gfz-potsdam.de (M. Förster), afield@aol.com (Y. I. Feldstein,), gromova@izmiran.ru (L. I. Gromova,).
[1] also at: Department of Physics and Technology, University of Bergen, Norway

1 Introduction

The group of four identical Cluster satellites performs plasma measurements in vast ranges of the Earth's magnetosphere and beyond since February 2001. The Electron Drift Instrument (EDI) onboard Cluster measures the 2-D drift velocity of artificially injected electrons perpendicular to the local geomagnetic field. EDI emits two low-intensity 1 keV electron beams and receives the returning beam after one or more gyrations in the surrounding magnetic field. Due to the cycloidic motion, the electron beam can be recorded only when fired in a particular direction, which is unambiguously determined by the intensity and direction of the plasma drift. The measurement principle requires a continuous tracking of the true changes for these firing directions. The drift vector is estimated by triangulation of the two beams or from the difference of their time-of-flight (*Paschmann et al.*, 2001).

The observed minimum drift velocity amounts to $\sim$1 km/s, which corresponds to $\sim$0.1 mV/m for a magnetic field strength of $\sim$100 nT in the magnetosphere. An important advantage of the EDI technique for measurements at high altitudes consists in its insensitivity to wake effects, which influences electric field measurements by means of plasma probes in low-density environments of the outer magnetosphere (*Eriksson et al.*, 2006). EDI performs electric field measurements with a time resolution of $\lesssim$10 Hz (depending on beam returns); for this study we use 1 minute average values only.

The satellites moved along an excentric, near-polar orbit with an apogee and perigee of initially $\sim$4 R_E and $\sim$19.6 R_E, respectively, and an orbital period of $\sim$57 hours. The orbital precession rate is such, that all magnetic local times (MLT) of both polar caps (above an invariant latitude $\Phi > \sim 74°$) are covered twice per year with observations. The spacecraft's velocity is about 3 to 4 km/s for typical overflights above the polar cap.

The distance between individual data points after their mapping from the magnetospheric measurement point into the ionosphere at $\sim$400 km altitude amounts to about $\sim$2 km in latitude and $\sim$20 km in longitude. Due to the precession constraints, the local time coverage of data points, mapped to magnetic latitudes $\Phi < \sim 74°$, changes with season. During summer months in the Northern Hemisphere (June-August), the daytime to afternoon sector is covered, while during the northern winter months (December-February) it is the nighttime to early morning sector. For the global coverage over all MLT, data of at least one full calendar year are needed.

The magnetic field vector are measured onboard Cluster by means of a three-component fluxgate magnetometer (FGM), which are mounted at 5 m radial booms. The measurement interval in various operative ranges spans

over ±4000 nT with a typical precision of 0.1 nT (*Balogh et al.*, 2001). For the mapping of the electric field measurements from the magnetosphere to the ionosphere we use the Tsyganenko-2001 model of the outer geomagnetic field (*Tsyganenko*, 2002a,b). The input parameter of this model comprises not only the actual values of solar wind velocity, density, and the components of the interplanetary magnetic field (IMF), but also their values of the preceding hour.

In the next Section 2 we will shortly explain the methodology of determining the spatio-temporal electric field pattern in dependence of the IMF orientation, as it was described in detail by the companion papers of *Haaland et al.* (2007), *Förster et al.* (2007), and *Förster et al.* (2008). These patterns are then presented in Section 3. Section 4 presents some estimations of approximative patterns, which were also used for the construction of a statistical ionospheric convection model that describe the dependencies on IMF B_y and B_z (*Förster et al.*, 2009). In Section 5 we illustrate our trials to derive the convection part that might be controlled by the IMF B_x component. In the Conclusions (Section 6) we finally summarize the main findings of this study.

2 Methodology to determine the ionospheric electric field pattern

The solar wind parameters and the IMF vector data were obtained from the ACE satellite near the L1 libration point upstream of the Earth and time shifted to represent the IMF conditions at the frontside magnetopause (at $X_{GSM} = 10$ RE) using the phase front propagation technique (*Weimer et al.*, 2003; *Haaland et al.*, 2006). It assumes the existence of "phase fronts", which can adopt any angle with respect to the solar wind velocity and parallel to which the adjacent IMF orientation is supposed to propagate toward the Earth.

The EDI/Cluster measurements are obtained far from the Earth's ionosphere. To derive the regularities of the ionospheric convection pattern, a mapping of the observations to the ionospheric level is presumed. Such a procedure presupposes usually the existence of equipotentiality along the geomagnetic field lines in correspondence with a geomagnetic field model (*Baker et al.*, 2004).

Assuming the spacecraft at a certain position X_1^m in the magnetosphere, its mapping point at 400 km altitude in the ionosphere X_1^i is uniquely determined by the model. Then the potential difference between X_1^m and the position X_2^m, which is located at a distance d^m in the magnetospheric drift vector direction $\vec{V}^m$, amounts to $\Delta\Phi^m = E^m d^m = V^m B^m d^m$, where E^m is the electric field in the magnetosphere, which is constant over the distance d^m, and B^m is the

magnetic field strength. The precision of electric field measurements of EDI in the magnetosphere is between 0.1 mV/m and 0.2 mV/m.

A distance d^m of the order of ∼1000 km was assumed in dependence on the magnetic field magnitude ratio in the ionosphere B^i and magnetosphere B^m, so that it results in d^i ∼50 km. The mapping of X_2^m to the ionospheric point X_2^i determines the value d^i, which is the projection of d^m into the ionosphere in magnitude and orientation. The potential difference over d^i is equal to $\Delta\Phi^i = E^i d^i = V^i B^i d^i$. Under the assumption of equipotentiality along the geomagnetic field lines, we have $\Delta\Phi^m = \Delta\Phi^i$, so that the electric field at ionospheric height amounts to $E^i = E^m d^m / d^i$.

The electric field at upper ionospheric heights can be obtained from the EDI measurements under the assumption that the geomagnetic field lines are frozen into the plasma flow (*Haaland et al.*, 2007). The time interval t^m to move the magnetic field line from point X_1^m over the distance d^m to X_2^m amounts to $t^m = d^m / V^m$, where V^m is the drift velocity in the magnetosphere as measured by EDI. The convection time t^i of the plasma flow over the distance d^i between the points X_1^i and X_2^i in the ionosphere, which are the projections of X_1^m and X_2^m, results in $t^i = d^i / V^i$. Under the frozen-in assumption we have $t^i = t^m$ and therefore $V^i = V^m (d^i / d^m)$. Throughout the paper we use ionospheric convection velocities V^i, obtained from EDI observations in the spacious magnetosphere under the assumption of the frozen-in condition of plasma flow.

3 Convection at high latitudes for different orientations of the IMF

The measured EDI electric field vectors, mapped into the high-latitude ionosphere and binned into 784 grid points within 32° of magnetic co-latitude range, were sorted and averaged with respect to the IMF orientation in the GSM y-z-plane into 8 sectors of 45° width each. The bins have 2° width in latitude and are variable in magnetic local time (MLT) in such a manner, that the bins' area are approximately of equal size with $\sim 5 \times 10^4 km^2$. The electric field grid is therefore equidistant in magnetic latitude (MLAT) and inhomogeneous in longitude (MLT).

The global convection pattern is established in terms of the electric potential distribution, Φ, based on the electric field data $\vec{E}$ at ionospheric level, related by the expression

$$\vec{E} = -\vec{v} \times \vec{B} = -\text{grad}\, \Phi. \tag{1}$$

The plasma drift vector grid pattern is thus fitted to a smoothed potential

IMF		$< B_x >$	$< B_y >$	$< B_z >$
Sector	direction	[nT]	[nT]	[nT]
0	B_z+	0.02	0.05	3.79
1	B_z+/B_y+	-1.54	3.13	2.66
2	B_y+	-2.57	4.48	0.01
3	B_z-/B_y+	-2.48	3.23	-2.87
4	B_z-	-1.46	-0.02	-4.82
5	B_z-/B_y-	2.19	-3.87	-3.30
6	B_y-	2.84	-5.02	0.00
7	B_z+/B_y-	1.90	-3.81	3.00

Table 1
Median values of IMF B_x, B_y, and B_z for the years 2001/02-2009/04.

distribution Φ by minimizing the quantity χ^2 given by

$$\chi^2 = \sum_{i=1}^{N} \mid \vec{E}_i + \text{grad } \Phi \mid^2 \tag{2}$$

For the analytic presentation of the potential in the high-latitude region, bounded toward the equator at 58° geomagnetic latitude, we used the spherical harmonic analysis (*Haines*, 1985). They were applied for each sector individually as function of geomagnetic co-latitude θ and MLT (via the azimuthal angle ϕ).

$$\begin{aligned} \Phi(\theta,\phi) = & \sum_{l=0}^{L} A_{l0}\ P_l^0(\cos\theta) \\ & + \sum_{l=0}^{L}\sum_{m=0}^{l} (A_{lm}\cos m\phi + B_{lm}\sin m\phi)\ P_l^m(\cos\theta) \end{aligned} \tag{3}$$

where P_l^m are the associated Legendre polynomials with degree l and order m of the harmonic polynomials, A_{lm} and B_{lm} are the real parts of the coefficients, uniquely determined from the $N \times K$ matrix. Here, N is the number of grid points and K the number of coefficients, determined by the number of the spherical harmonics used ($L = 8$ or 10 in our case), so that $K = (L+1)^2$.

The spatio-temporal distribution of the electric potential at high latitudes were obtained by accumulating data of convection intervals with well-established IMF orientation (cf. *Haaland et al.*, 2007). Fig. 1 shows such potential distributions for 8 different orientations (sectors) of the IMF near the magnetopause. The panels are drawn in Altitude Adjusted Corrected Geomagnetic (AACGM)

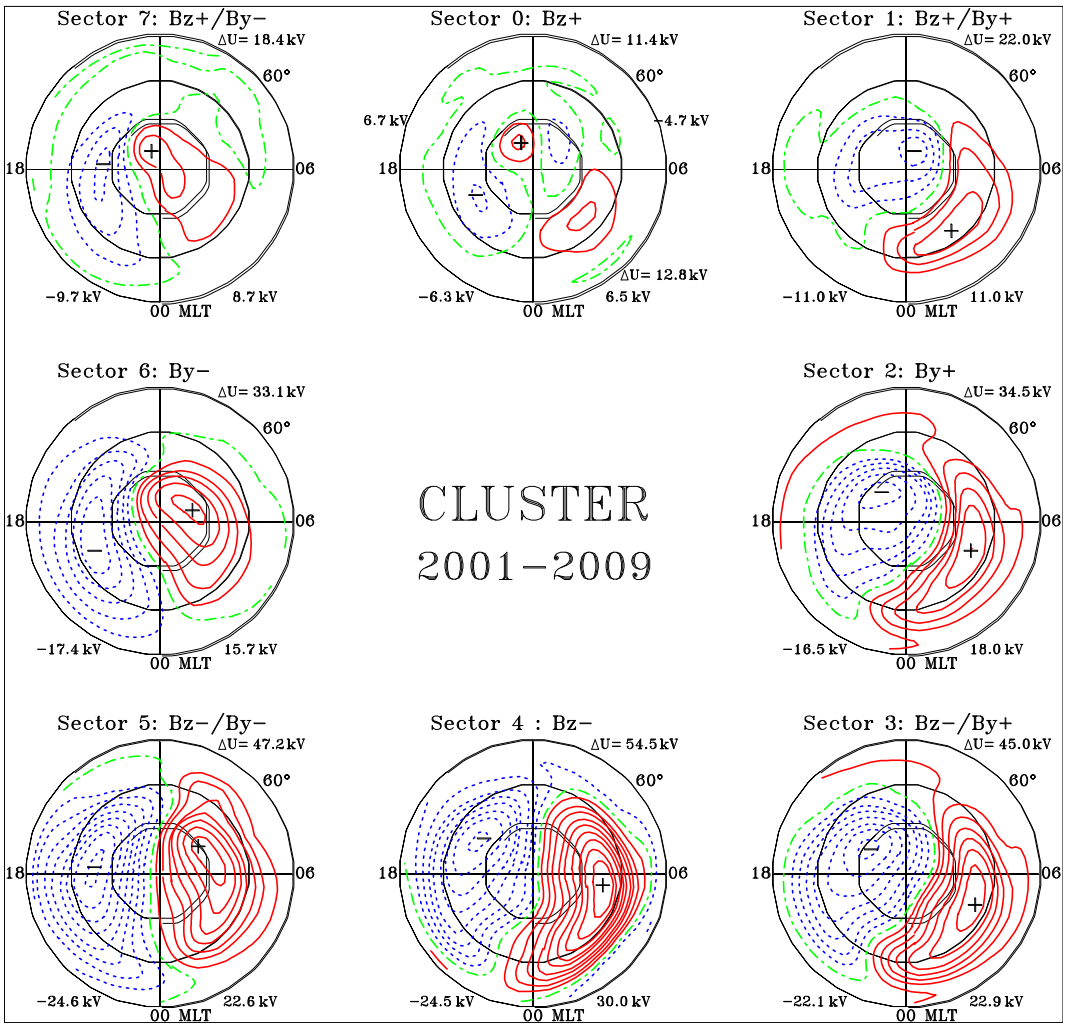

Fig. 1. Electric potential patterns obtained from Cluster C1-C3 EDI observations in the Northern Hemisphere as a function of magnetic latitude and magnetic local time for 8 IMF clock-angle orientations (sectors). The positions of maximum and minimum values are indicated by "+" and "-" sign, respectively, and their values are shown at the bottom line of each panel. The total cross-polar cap potential difference ΔU is indicated at the upper right corner for each sector. For sector 0 (IMF $B_z > 0$), the maximum and minimum values for the high-latitude dayside cells are shown additionally. Positive and negative potential values are displayed by continuous and dashed lines, respectively, while their spacing is 3 kV.

coordinates with 60° at the outer border versus MLT using EDI data from the interval February 2001 to April 2009. Table 1 lists the mean values of the IMF components for the data points used in each sector.

The isolines of Fig. 1 are plotted in AACGM (Altitude Adjusted Corrected Geomagnetic) coordinates with a 3 kV spacing, where the outer border of the dials is at 60° magnetic latitude. The EDI measurements occured predominantly during moderate IMF vector amplitudes with median values of ∼4 nT

to 5 nT. The sector width is 45° of IMF angle orientation in the GSM y-z-plane with 8 distinct sectors (from sector 0 to sector 7), which are also 45° apart from each other, shifted in clockwise direction. For southward IMF (sector 4), the convection pattern consists of two cells, the foci of which are located at 73° magnetic latitude on the morning and at 75° on the evening side with antisolar (from the dayside to the nightside) directed convection across the polar cap. The separation line between the two cells is approximately oriented along the noon to midnight meridian. The cross-polar cap potential difference between the cell pair foci amounts to $\Delta U = 54.5$ kV, which is the maximum value of all 8 IMF orientations (sectors).

For east-west orientation of the IMF (sector 2 for $B_y > 0$ and sector 6 for $B_y < 0$), the two-cell convection pattern is kept. In the polar cap, there takes place a deformation of the plasma convection cells: the area of the evening/morning side cell increases in sectors 2/6 in case of the Northern Hemisphere (mirror symmetric at the Southern Hemisphere). The zero potential line is shifted simultaneously toward the morning/evening side.

For northward directed IMF (sector 0), there appears a further pair of convection cells at the dayside high latitudes with $\Delta U \sim 11.4$ kV and sunward directed convection (from the nightside toward the dayside) between them, additionally to the two main (nightside) cells with $\Delta U \sim 12.8$ kV. According to Fig. 1, the main cell potential drop decreases steadily when turning from sector 4 to sector 0. The potential difference between the two cell pairs of sector 0 differs only by 1.4 kV.

4 Estimation of the potential accuracy and the convection model

Table 2 lists the potential differences ΔU for various data sets, which allows to evaluate the variation of these cross-polar potential drops in dependence on the length of the data sample interval and the degree of spherical harmonics (8 versus 10) according to equation (3). For this analysis we used partly data given in the public literature (*Haaland et al.*, 2007; *Förster et al.*, 2009; *Haaland et al.*, 2009).

For the data sets of the full interval 2001-2009 with both degree 8 and 10 of spherical harmonics, we get practically no difference for all 8 sectors. The scatter of the ΔU values is confined to 0.3 kV for the main cells and 0.1 kV for the minor dayside cells at high latitudes (sector 0).

The summer values ΔU are taken from Table 2 of *Förster et al.* (2009). In order to get global data coverage, there were used both Northern (March to September) and Southern Hemisphere (September to March) values. The

IMF Sector	$\Delta U(kV)$ 2001-2006 (8 harmonic)[1]	$\Delta U(kV)$ 2001-2009 (8 harmonic)[2]	$\Delta U(kV)$ 2001-2009 (10 harmonic)[3]	$\Delta U(kV)$ 2001-2008,summer (10 harmonic)[4]
0	12.8 (dayside) 14.3 (nightside)	11.4 12.8	11.4 12.8	11.0 13.6
1	27.5	21.5	22.0	24.1
2	40.6	34.2	34.5	37.5
3	54.3	45.0	45.0	54.2
4	61.9	54.2	54.5	58.1
5	51.3	47.4	47.2	43.5
6	33.5	33.1	33.1	37.7
7	18.3	18.9	18.4	21.5

Table 2
Cross-polar cap potential ΔU (kV) between the high-latitude convection foci at the Northern Hemisphere for Cluster/EDI data of ([1]) *Haaland et al.* (2007), ([2]) *Haaland et al.* (2009), ([3]) this study and ([4]) *Förster et al.* (2009).

latter subset was projected into the Northern data set with inverted sign of the IMF B_y component. The differences of the potential drops between the full year set and the summer set are of the order of a few kV with an average of ∼4 kV difference, where the higher values are for all sectors of the summer data set, except of sector 5. The high-latitude dayside pair of sector 0 differs only by $\Delta U = 0.4$ kV, the three northward directed IMF sectors (7, 0, and 1) have an average difference of $\Delta U = 2.2$ kV, and the three southward directed IMF sectors (3-5) scatter around ~ 6.0 kV.

The augmentation of the data volume from about 5 years (02/2001–03/2006) to about 8 years (02/2001–04/2009) is accompanied by a change of the cross-polar cap potential differences: it diminishes by 1.4 kV for the high-latitude dayside cells, by 7.3 kV for southward, and by 2.2 kV for northward IMF.

The statistical convection model as proposed by *Förster et al.* (2009) based on Cluster EDI measurements proposes a linear relationship of the potential with the IMF B_y and B_z components:

$$U(\theta, \phi, B_y, B_z) = U_0(\theta, \phi) + \hat{U}_{\pm y}(\theta, \phi) \cdot (\pm B_y) + \hat{U}_{\pm z}(\theta, \phi) \cdot (\pm B_z) \qquad (4)$$

where U_0 (in kV) represents a constant term which is independent of the IMF, while the terms $\hat{U}_{\pm y}$ and $\hat{U}_{\pm z}$ (in kV/nT) describe the linear dependencies on the IMF B_y and B_z components, respectively, normalized to 1 nT variations, which can be different for different signs. The plasma drift velocity measurements confined mainly to moderate B_y and B_z magnitudes (see Table 1), which

justifies the use of linear relationships. Such a decomposition of the potential pattern dependencies has been used previously already by, e.g., *Feldstein and Levitin* (1986), *Papitashvili and Rich* (2002) and *Kabin et al.* (2003).

Fig. 2 shows the elements of Basic Convection Pattern (BCP): U_0 (upper left panel), $\hat{U}_{\pm y}$ (lower right panel for $B_y = \pm 1$ nT, drawn here for $B_y = +1$ nT), $\hat{U}_{+z}$ (upper right panel with $B_z = +1$ nT) and, finally, $\hat{U}_{-z}$ (lower left panel with $B_y = -1$ nT). The BCP elements are calculated from the summation of various potential pattern of the sectors in Fig. 1: The U_0 background potential for vanishing IMF B_y and B_z components (upper left panel) is derived as the sum of sectors 2 and 6 of Fig. 2, while the B_y dependence (lower right panel) is derived from their difference, normalized to $\Delta B_y = 1$ nT. $\hat{U}_{+z}$ and $\hat{U}_{-z}$ are determined as potential differences between sector 0 or sector 4, respectively, and the U_0 background potential, normalized to $\Delta B_z = +1$ nT or -1 nT.

The IMF-independent part of the potential, U_0, complies with a two-cell pattern with antisolar convection over the polar cap. An analoguous two-cell pattern displays the $\hat{U}_{-z}$ potential. The $\hat{U}_{+z}$ potential appears as two-cell pattern with a concentration of the isolines in the dayside high-latitude region, where the convection is sunward directed. The $\hat{U}_{\pm y}$ potential, finally, corresponds to a one-cell convection within the polar cap, the focus of which is close to its center. In the Northern Hemisphere, the plasma convection is clockwise for positive B_y+ and counterclockwise for negative B_y-.

The BCP elements can be calculated also with other combinations of the 8 IMF sector potential distributions. Some results of such calculations are presented in Fig. 3. The headline of each panel shows the relation and IMF sectors used for the calculation of each of the BCP elements. The potential values of the foci are indicated below each panel and the total potential difference on the upper right. For the calculation of the BCP elements we used the following relations:

$$\begin{aligned}
\hat{U}_{z-} &= (sector3 + sector5 - 2U_0)/6.17 \\
\hat{U}_{z+} &= (sector1 + sector7 - 2U_0)/5.66 \\
\hat{U}_{y+} &= (sector3 - sector5)/7.10 \quad or \\
\hat{U}_{y+} &= (sector1 - sector7)/6.94
\end{aligned} \tag{5}$$

Figures 2 and 3 represent BCP elements, which are controlled by the IMF components B_y and B_z obtained independently from different original data. They are practically identical with respect to the following: number and orientation of the convection cells, position of its foci, potential difference between the foci, which only differ by 0.7 kV for $\hat{U}_{-z}$, by 0.5 kV for $\hat{U}_{+z}$, and for the cells $\hat{U}_{\pm y}$ within the polar cap by 0.3 kV. This good agreement be-

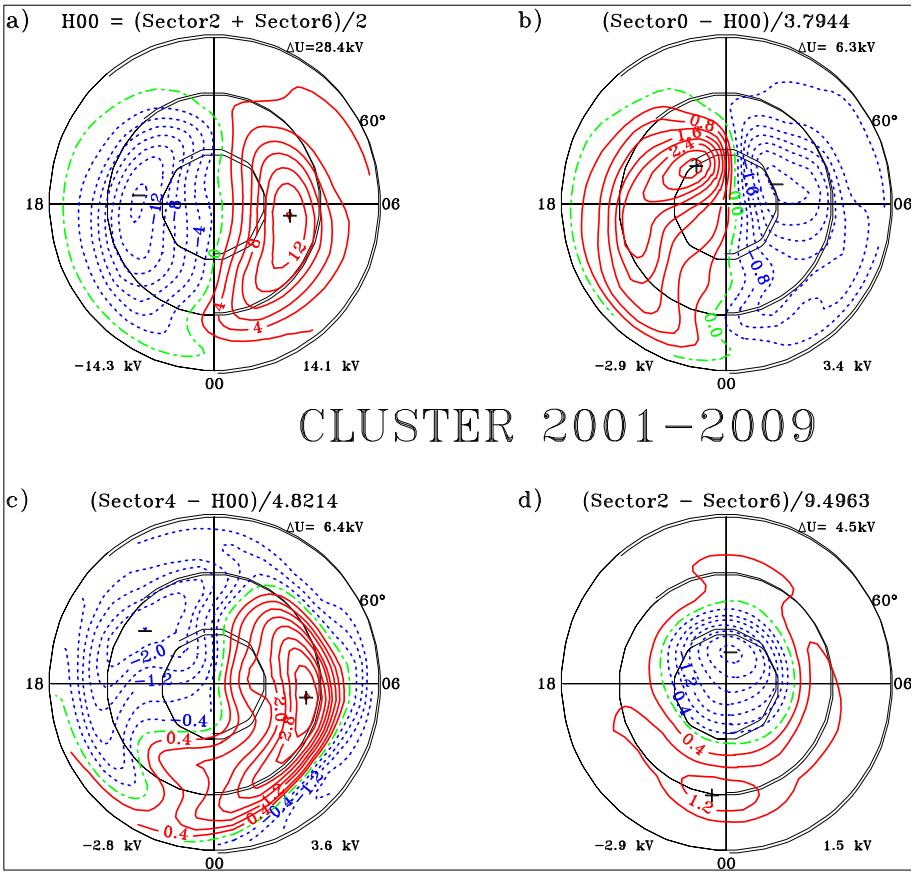

Fig. 2. This figure shows the elements of the Basic Convection Patterns (BCPs), derived from Cluster EDI observations for various orientations of the IMF, as presented in Fig. 1. The entirety of them constitutes the ionospheric convection model in dependence of the IMF: a) the part of potential distribution, which is independent of IMF B_z and B_y; b) isolines of the potential contribution for the positive B_z value range, normalized to $B_z = +1$ nT; c) the same for the negative B_z value range, i.e., $B_z = -1$ nT; d) potential distribution for the normalized $B_y = 1$ nT. The relations to calculate the respective elements are denoted above each panel.

tween the BCP elements lends credence to their validity, because they result in approximately the same pattern, although they were derived from different, independent plasma drift measurements of EDI.

The spatio-temporal convection pattern and the cross-polar cap potential drop ΔU at high latitudes were obtained from EDI data for different IMF orientations within sectors of $\alpha = 45°$ conus angle width. A compelling question is therefore, whether the convection pattern changes for smaller conus angles α. *Förster et al.* (2008) considered the pattern changes (for near-northward IMF) in steps of 5° IMF orientation, while keeping the 45° cone width. Here, we estimated the influence of varying α on the characteristics and intensity of the high-latitude convection, when analysing EDI data at both hemispheres from the time interval Feb 2001 to Apr 2009. We used 8th order harmonics for

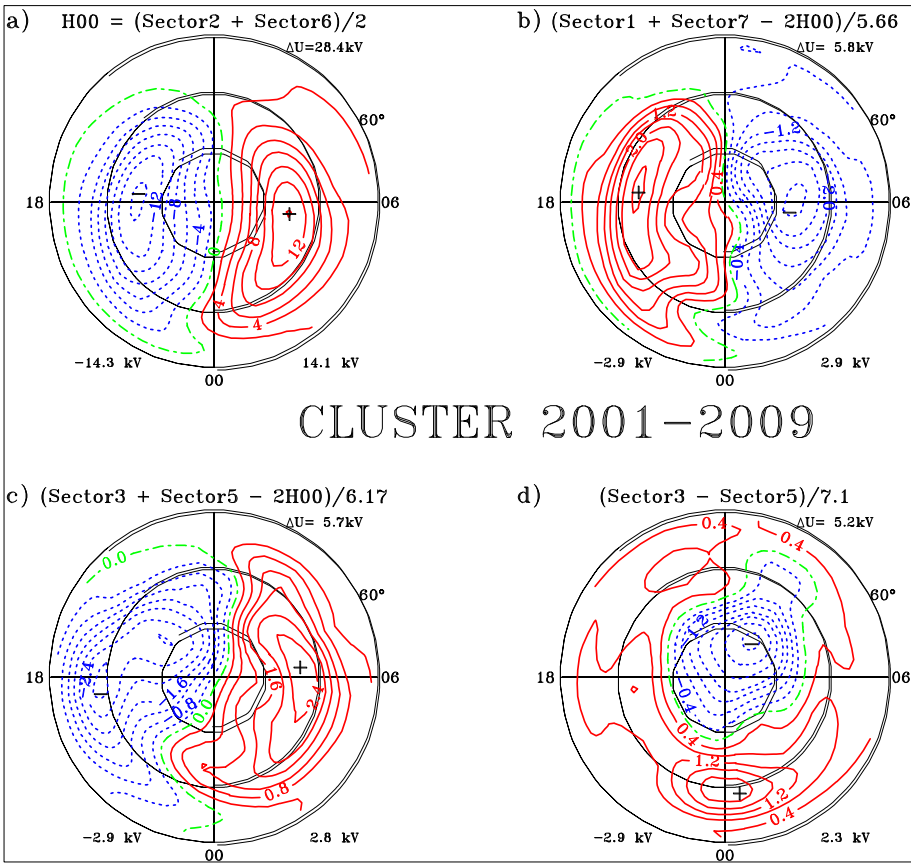

Fig. 3. The same as in Fig. 2, but using the relations given in (5) for the calculation of the BCPs instead of those shown in Fig. 2.

the analysis and diminished $\alpha = 45°$ in steps of 10°. The convection characteristics practically kept unchanged down to $\alpha = 10°$, i.e., the two-cell plasma convection pattern of the main cells in the morning and evening side persisted for all sectors and an additional pair of high-latitude dayside cells appeared for northward IMF (sector 0). The data coverage downgraded continuously with diminishing angle α, in particular for magnetic latitudes $< 75°$, and changed for the worse when $\alpha = 7.5°$, where even the characteristics of the derived potential pattern changed. When diminishing α from 45° to 10°, the cross-polar cap potential difference ΔU stayed near 20 ± 2 kV for the northward oriented sectors 1 and 7, and at the lower level of 13 ± 2 kV for sector 0. For the east-west oriented IMF, ΔU kept within 35 ± 3 kV for sectors 2 and 6, while it was 52 ± 5 kV for the southward IMF sectors 3 and 5 and 55 ± 6 kV for sector 4. The reduction of the cone angle α from 45° to 10° does therefore not lead to any significant change in the convection characteristics nor changes its intensity by more than 10%.

5 The IMF B_x component and the plasma convection in the high-latitude ionosphere

There are different, even completely contrary opinions about the influence of the IMF B_x component on geophysical processes at high latitudes in the public literature. *Yahnin and Sergeev* (1981); *Crooker* (1986); *Cowley et al.* (1991); *Belenkaya* (1998); *Blomberg et al.* (2005); *Alexeev et al.* (2007); *Newell et al.* (2009); *Peng et al.* (2010) advance the view that B_x has an appreciable influence, while the studies of *Levitin et al.* (1982) and *Newell et al.* (1989) couldn't find any significant influence of this IMF component on the high-latitude current systems. The difficulty to assign any IMF B_x dependence is due to the essential sector structure of the IMF in the ecliptic plane, which consists of two different sectors, in each of which the B_x and B_y components of the IMF vector have opposite signs. Analysing the geomagnetic variations in the near-polar region, *Friis-Christensen et al.* (1972) and *Sumaruk and Feldstein* (1973) concluded, that the sector structure effect is dominated by the B_y component. This conclusion was based on event studies of geomagnetic variations in the polar cap and their correlation with the IMF vector components during intervals, when the sector structure was unsettled and these two vector components had the same sign. Their results are nowadays generally accepted and all published high-latitude statistical convection models include only the dependence on the IMF B_y and B_z components to describe the spatio-temporal convection pattern.

The large amount of EDI drift measurements at high latitudes with the Cluster satellites during more than 8.5 years allows us to re-investigate the influence of the IMF B_x component on the ionospheric plasma convection. For this purpose, we have divided the data into two subsets of about the same size with $B_x > 0$ (IMF vector directed toward the sun) on the one hand and $B_x < 0$ (IMF away from the sun) on the other. Each subset has then sorted for the same 8 sectors of IMF orientation in the GSM y-z-plane as before and the electric potential distributions in the ionosphere at 400 km altitude have been calculated based on the same method as described in Sections 2 and 3 above. The characteristics of the potential distribution in all 8 sectors resemble the convection pattern shown in Fig. 1, which confirms that even one half of the data is sufficient to get stable potential distributions. The mean IMF B_x amplitude varies in the different sectors from about 2 nT to 4 nT; the lower values of $\sim$2 nT are met in the sectors, where $< B_x >$ and $< B_y >$ have the same sign, while the $\sim$4 nT values are in sectors with opposite sign.

Table 3 shows the cross-polar cap potential difference between the morning and the evening side foci of all 8 sectors for both the Northern and the Southern Hemisphere separately for $B_x > 0$ and $B_x < 0$ conditions. One may conclude from these data that not only the general characteristics of the con-

IMF orientation		$\Delta U(kV)$ North Hemisphere		$\Delta U(kV)$ South Hemisphere	
Sector		$B_x > 0$	$B_x < 0$	$B_x > 0$	$B_x < 0$
0	B_z+	15.5	15.4	11.5	11.8
1	B_z+/B_y+	21.8	24.6	22.9	23.4
2	B_y+	35.4	34.0	37.9	37.9
3	B_z-/B_y+	50.8	44.5	47.2	48.2
4	B_z-	58.5	54.6	52.5	57.4
5	B_z-/B_y-	44.2	59.4	49.5	49.7
6	B_y-	32.9	35.9	33.4	34.8
7	B_z+/B_y-	17.7	24.2	21.9	20.6

Table 3
Cross-polar cap potential ΔU between the main convection foci in kV for Cluster/EDI data of the years 2001-2009, sorted separately for IMF directed toward the Sun ($B_x > 0$) and away from the Sun ($B_x < 0$).

vection pattern is kept, but also the regularity of the cross-polar cap potential difference changes: ΔU increases monotonically from sector 0 to sector 4 and reduces again for negative B_y values from sector 4 to sector 0. At the Southern Hemisphere this regularity is valid throughout, while for the Northern there is one exception for sector 5 with negative $B_x < 0$. We suppose that this exception may be explained by an insufficient number of data points, firstly, because of the orbital characteristics of the Cluster satellites with its apogee turning southward, which preferred Southern Hemisphere data, and secondly, because of the generally smaller number of data points with equal sign B_x and B_y. The compilation of ΔU values of both hemispheres with opposite $<B_x>$ orientations (Table 3) doesn't give significant evidence for a B_x dependence of the cross-polar potential drop.

We made further an attempt to find out parts of the high-latitude convection, which might be controlled by IMF B_x. As described below, this attempt considered two different methods which are based on different assumptions.

The first method draws upon the presumption that the IMF B_x component does not have an effect for the convection in case of equally directed B_x and B_y, i.e., at the Northern Hemisphere and $B_x > 0$ this is the case for sectors 1, 2, and 3, while for $B_x < 0$ this is valid for sectors 5, 6, and 7. In the further calculations we consider only sectors 2 and 6, where the influence of IMF B_z is practically vanishing and the convection pattern becomes therefore more simple.

The second method draws upon the circumstance, that the Earth's dipole

Element of BCP	Northern Hemisphere Method 1	Method 2	Southern Hemisphere Method 1	Method 2
U_0	30.4	29.5	33.3	30.9
$\hat{U}_{+y}$	-2.9	-3.0	2.8	2.5

Table 4
Potential difference ΔU in kV for the BCP U_0 and $\hat{U}_{+y}$, based on Cluster EDI data for the years 2001-2009.

magnetic field lines over the northern polar cap region have an opposite direction to the IMF field lines for $B_x < 0$, but over the southern for $B_x > 0$. An opposite direction of the IMF and the magnetospheric tail magnetic field constitutes a favourable condition for the penetration of solar wind plasma into the polar cap region (*Newell et al.*, 2009). An enhanced flow of soft energetic particles can likewise affect the convection due to an increased level of ionisation of the upper atmosphere.

More details about the methodology of the various trials to deduce B_x dependent parts of convection from Cluster/EDI data and the results obtained are described in *Förster et al.* (2011).

Accomplishing the above relations, we get the convection pattern for the IMF-independent element U_0, as well as the elements, which are controlled by the IMF $\pm B_y$ and $\pm B_x$ components ($\hat{U}_{\pm y}$ and $\hat{U}_{\pm x}$, respectively). The U_0 element describes in all cases a two-cell convection with foci on the morning and on the evening side and an antisolar convection across the polar cap, while the $\hat{U}_{\pm y}$ element specify a one-cell convection within the polar cap, the focus of which is situated close to the geomagnetic pole with a circulation at the Northern/Southern Hemisphere in counter-clockwise(CCW)/clockwise(CW) direction for $B_y > 0$ and CW/CCW for $B_y < 0$. The cross-polar cap potential drops ΔU for U_0 and the potential values of the $\hat{U}_{+y}$ elements are given in Table 4.

The characteristics of the potential pattern and the ΔU values of the BCP elements U_0 and $\hat{U}_{\pm y}$ (Table 4) show a good agreement for both methods as well as with the previously determined values according to *Förster et al.* (2009) or those in Fig. 2 with $\Delta U(U_0) = 28.4$ kV and 30.0 kV and $\Delta U(\hat{U}_{+y}) =$ -2.9 kV and -3.0 kV, respectively. Such a good correspondence can serve as an additional valid argument in favour of the legitimacy of the presumtions adopted for the calculation of the BCPs.

The characteristics and the intensity of the convection pattern deduced for $\hat{U}_{\pm x}$ is not that clear. There is no regular, systematic convection pattern, but rather some small randomly distributed vortices. The isolines are very irregular and the vortices have peak values, which are several times smaller than those related to the IMF B_y and B_z components. There didn't appear specific

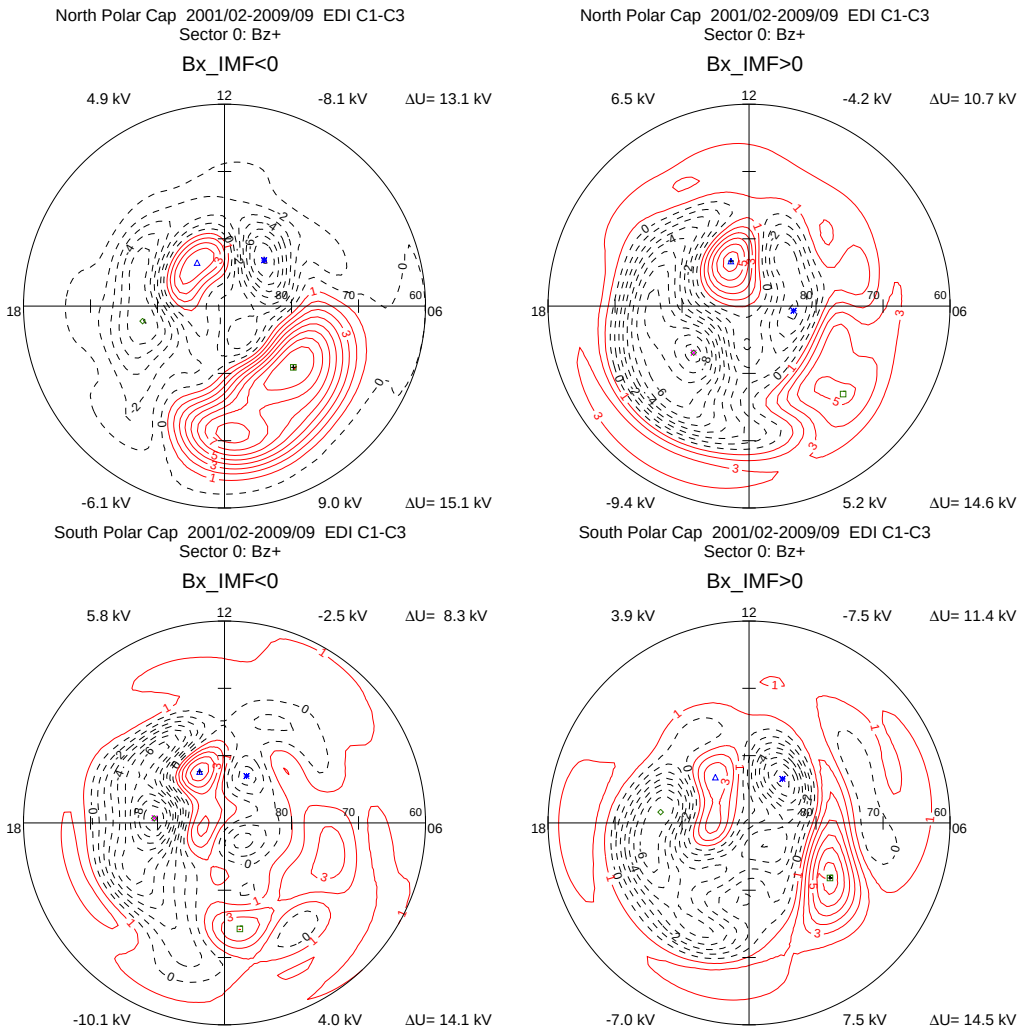

Fig. 4. High-latitude convection pattern of Sector 0 (IMF $B_z > 0$) obtained from Cluster C1-C3 EDI observations during the years 2001/02-2009/09. The numbers indicate the peak potential values of the corresponding foci (as for Sector 0 in Fig. 1). The panels show a) North hemisphere with IMF $B_x < 0$; b) North hemisphere with $B_x > 0$; c) South hemisphere with $B_x < 0$ and d) South hemisphere with $B_x > 0$.

distributions, which could be related to the sign of IMF B_x or to hemispheric differences. We couldn't therefore reveal any conclusive evidences for the presence of an IMF B_x dependence in the convection pattern, its characteristics or intensity for the given situation.

On the other hand, the analysis of the potential drops between the high-latitude dayside cells, as they appear for IMF $B_z > 0$ (sector 0), provides some reason to assume a slight IMF B_x dependence.

Figure 4 shows the potential pattern in sector 0 for the Northern and Southern hemisphere for opposite orientations of IMF B_x. There appear 4-cell convection patterns during all these situations with a pair of sunward directed

cells at the dayside with the foci before and after midday at geomagnetic latitudes between 82° and 84°. The potential drop between the dayside high-latitude foci shows some correlation with the IMF B_x component. It is larger for situations of anti-parallel orientation of the geomagnetic field line in the magnetospheric tail and the IMF B_x component. For the Northern polar cap this corresponds to an IMF orientation with $B_x < 0$ and for the Southern polar cap to $B_x > 0$.

6 Conclusions

Based on the complemental analyses of the present study we conclude:

1. The elements of the basic convection pattern (BCP), which were derived by different methods and by using independent data, are qualitatively identical in shape and orientation of the convection cells as well as in the position of their focal points. The cross-polar potential difference in the Northern Hemisphere for the IMF-independent part amounts to $\Delta U(B_{00}) = 29.4 \pm 0.7\ kV$, while the IMF-dependent components of the BCPs add up to $\Delta U(B_y = +1\ nT) = -2.8 \pm 0.2\ kV$ for $B_y > 0$, $\Delta U(B_z- = -1\ nT) = 6.0 \pm 0.3\ kV$ for $B_z < 0$, and $\Delta U(B_z+ = +1\ nT) = 6.0 \pm 0.2\ kV$ for $B_z > 0$. The conformance of the BCP elements in the limits of a few percent lends credence to the correctness of their quantitive estimation, because they were obtained from independent plasma drift measurements of EDI.

2. The methodology and the results of the spatio-temporal potential distribution, which was obtained by *Förster et al.* (2009) are affirmed also with respect to a) an upgrading of the spherical harmonics from 8th to 10th order in the modelling; b) the reduction of the sector's IMF conus angle width from 45° to 10°.

3. The potential difference between the pairs of dayside high-latitude convection cells of Sector 0 (IMF $B_z > 0$) appears to be larger for situations of an anti-parallel orientation between the magnetic field of the magnetospheric tail and the adjacent solar wind. On the other hand, there are no significant evidences for an IMF B_x dependence of the convection pattern both in shape and intensity of the main (nighttime) cells.

Acknowledgement
Work at GFZ German Research Centre for Geosciences Potsdam (M. F.) was supported by Deutsche Forschungsgemeinschaft (DFG). Research at the University of Bergen (S.E.H.) was supported by the Norwegian Research Council. We thank the ACE SWEPAM and MAG instrument teams and the ACE Science Center for providing the ACE data.

References

Alexeev, I. I., E. S. Belenkaya, S. Y. Bobrovnikov, V. V. Kalegaev, J. A. Cummnok, and L. G. Blomberg, Magnetopause mapping to the ionosphere for northward IMF, *Ann. Geophys.*, *25*(12), 2615–2625, 2007.

Baker, J. B., R. A. Greenwald, J. M. Ruohoniemi, M. Förster, G. Paschmann, E. F. Donovan, N. A. Tsyganenko, J. M. Quinn, and A. Balogh, Conjugate comparison of SuperDARN and Cluster EDI measurements of ExB plasma drift, *J. Geophys. Res.*, *109*(A1), A01209, doi:10.1029/2003JA009912, 2004.

Balogh, A., C. M. Carr, M. H. Acua, M. W. Dunlop, , T. J. Beek, P. Brown, K.-H. Fornacon, E. Georgescu, K.-H. Glassmeier, J. Harris, G. Musmann, T. Oddy, and K. Schwingenschuh, The Cluster magnetic field investigation: overview of in-flight performance and initial results, *Ann. Geophys.*, *19*(10/12), 1207–1217, 2001.

Belenkaya, E. S., High-latitude ionospheric convection patterns dependent on the variable IMF orientation, *J. Atmos. Sol.–Terr. Phys.*, *60*(13), 1343–1354, 1998.

Blomberg, L. G., J. A. Cumnock, I. I. Alexeev, E. S. Belenkaya, S. Y. Bobrovnikov, and V. V. Kalegaev, Transpolar aurora: time evolution, associated convection patterns, and a possible cause, *Ann. Geophys.*, *23*(5), 1917–1930, 2005.

Cowley, S. W. H., J. P. Morelli, and M. Lockwood, Dependence of convective flows and particle precipitation in the high-latitude dayside ionosphere on the X and Y components of the interplanetary magnetic field, *J. Geophys. Res.*, *96*, 5557–5564, 1991.

Crooker, N. U., An evolution of antiparallel merging, *Geophys. Res. Lett.*, *13*(10), 1063–1066, 1986.

Eriksson, A. I., M. André, B. Klecker, H. Laasko, P.-A. Lindqvist, F. Mozer, G. Paschmann, A. Pedersen, J. Quinn, R. Torbert, K. Torkar, and H. Vaith, Electric field measurements on Cluster: Comparing the double-probe and electron drift techniques, *Ann. Geophys.*, *24*, 275–289, 2006.

Feldstein, Y. I., and A. E. Levitin, Solar wind control of electric fields and currents in the ionosphere, *J. Geomag. Geoelectr.*, *38*(11), 1143–1182, 1986.

Förster, M., G. Paschmann, S. E. Haaland, J. M. Quinn, R. B. Torbert, C. E. McIlwain, H. Vaith, P. A. Puhl-Quinn, and C. A. Kletzing, High-latitude plasma convection from Cluster EDI: Variances and solar wind correlations, *Ann. Geophys.*, *25*(7), 1691–1707, 2007.

Förster, M., S. E. Haaland, G. Paschmann, J. M. Quinn, R. B. Torbert, H. Vaith, and C. A. Kletzing, High-latitude plasma convection during Northward IMF as derived from in-situ magnetospheric Cluster EDI measurements, *Ann. Geophys.*, *26*(9), 2685–2700, 2008.

Förster, M., Y. I. Feldstein, S. E. Haaland, L. A. Dremukhina, L. I. Gromova, and A. E. Levitin, Magnetospheric convection from Cluster EDI measurements compared with the ground-based ionospheric convection model IZMEM, *Ann. Geophys.*, *27*(8), 3077–3087, 2009.

Förster, M., Y. I. Feldstein, L. Gromova, L. A. Dremukhina, A. E. Levitin, and S. E. Haaland, Plasma convection in the high-latitude ionosphere deduced from Cluster EDI data and the IMF B_x component, in *Proceedings of the XXXIV. Annual Seminar, Apatity, Physics of Auroral Phenomena*, vol. 34, edited by A. G. Yahnin, Kola Science Centre, Russian Academy of Science, in press, 2011.

Friis-Christensen, E., K. Laasen, J. Wilhjelm, J. M. Wilcox, W. Gonzales, and D. S. Colburn, Critical component of the Interplanetary Magnetic Field responsible for large geomagnetic effects in the polar cap, *J. Geophys. Res.*, *77*(19), 3371–3376, 1972.

Haaland, S. E., G. Paschmann, and B. U. Ö. Sonnerup, Comment on "A new interpretation of Weimer et al.'s solar wind propagation delay technique" by Bargatze et al., *J. Geophys. Res.*, *111*, A06102, doi:10.1029/2005JA011376, 2006.

Haaland, S. E., G. Paschmann, M. Förster, J. M. Quinn, R. B. Torbert, C. E. McIlwain, H. Vaith, P. A. Puhl-Quinn, and C. A. Kletzing, High-latitude plasma convection from Cluster EDI measurements: Method and IMF-dependence, *Ann. Geophys.*, *25*(1), 239–253, 2007.

Haaland, S. E., M. Förster, G. Paschmann, R. B. Torbert, and H. Vaith, High-latitude plasma convection from Cluster EDI measurements: North-South asymmetries, in *AGU 2009 Fall Meeting, Session SM07*, San Francisco, 2009.

Haines, G. V., Spherical cap harmonic analysis, *J. Geophys. Res.*, *90*(B3), 2583–2591, 1985.

Kabin, K., R. Rankin, R. Marchand, T. I. Gombosi, C. R. Clauer, A. J. Ridley, V. O. Papitashvili, and D. DeZeeuw, Dynamic response of Earth's magnetosphere to By reversals, *J. Geophys. Res.*, *108*(A3), 1132, doi: 10.1029/2002JA009480, 2003.

Levitin, A. E., R. G. Afonina, B. A. Belov, and Y. I. Feldstein, Geomagnetic variations and field-aligned currents at northern high-latitudes and their relations to solar wind parameters, *Philos. Trans. Royal Soc.*, *A304*, 253–301, 1982.

Newell, P. T., C.-I. Meng, D. G. Sibeck, and R. Lepping, Some low-altitude cusp dependencies on the Interplanetary Magnetic Field, *J. Geophys. Res.*, *94*(A7), 8921–8927, 1989.

Newell, P. T., K. Liou, and G. R. Wilson, Polar cap particle precipitation and aurora: Review and commentary, *J. Atmos. Sol.–Terr. Phys.*, *71*(2), 199–215, 2009.

Papitashvili, V. O., and F. J. Rich, High-latitude ionospheric convection models derived from Defense Meteorological Satellite Program ion drift observations and parameterized by the interplanetary magnetic field strength and direction, *J. Geophys. Res.*, *107*(A8), 1198, doi:10.1029/2001JA000264, 2002.

Paschmann, G., J. M. Quinn, R. B. Torbert, H. Vaith, C. E. McIlwain, G. Haerendel, O. H. Bauer, T. M. Bauer, W. Baumjohann, N. Cornilleau-

Wehrlin, W. Fillius, M. Förster, S. Frey, E. Georgescu, S. S. Kerr, C. A. Kletzing, H. Matsui, P. Puhl-Quinn, and E. C. Whipple, The Electron Drift Instrument on Cluster: Overview of first results, *Ann. Geophys.*, *19*, 1273–1288, 2001.

Peng, Z., C. Wang, and Y. Q. Hu, Role of IMF Bx in the solar wind-magnetosphere-ionosphere coupling, *J. Geophys. Res.*, *115*, A08224, doi: 10.1029/2010JA015454, 2010.

Sumaruk, P. V., and Y. I. Feldstein, Sector structure of the interplanetary magnetic field and the magnetic variations in the near-polar region (in Russian), *Kosm. Issled.*, *11*, 155–160, 1973.

Tsyganenko, N. A., A model of the near magnetosphere with a dawn-dusk asymmetry 1. Mathematical structure, *J. Geophys. Res.*, *107*(A8), 1179, doi:10.1029/2001JA000219, 2002a.

Tsyganenko, N. A., A model of the near magnetosphere with a dawn-dusk asymmetry 2. Parameterization and fitting to observations, *J. Geophys. Res.*, *107*(A8), 1176, doi:10.1029/2001JA000220, 2002b.

Weimer, D. R., D. M. Ober, N. C. Maynard, M. R. Collier, D. J. McComas, N. F. Ness, C. W. Smith, and J. Watermann, Predicting interplanetary magnetic field (IMF) propagation delay times using the minimum variance technique, *J. Geophys. Res.*, *108*(A1), 1026, doi:10.1029/2002JA009405, 2003.

Yahnin, A. G., and V. A. Sergeev, Polar cap aurora: Dependence on IMF orientation and substorm; certain pecularities of morphology (in Russian), in *Aurorae and airglow*, vol. 28, pp. 27–34, Nauka, Moscow, 1981.